Manipulation and exchange of light with orbital angular momentum in quantum-dot molecules

Mahboubeh Mahdavi, Zahra Amini Sabegh, Mohammad Mohammadi, and Mohammad Mahmoudi [*]

Department of Physics, University of Zanjan, University Blvd., 45371-38791 Zanjan, Iran

Hamid Reza Hamedi [†]

Institute of Theoretical Physics and Astronomy, Vilnius University, Saulėtekio 3, Vilnius LT-10257, Lithuania

We study the interaction of laser pulses carrying orbital angular momentum (OAM) with structural asymmetry quantum-dot molecules characterized by four energy levels. We demonstrate how the interdot tunneling endows exchange of optical vortices between different frequencies. We consider a case where a weak probe beam has an optical vortex and thus has a zero intensity at the center. The presence of tunneling coupling generates an additional weak laser beam with the same vorticity as that of the incident vortex beam. We analyze conditions for the vortex of the initial beam to be transferred efficiently to the generated beam. The propagation of Laguerre-Gaussian (LG) beams possessing OAM states characterized by both azimuthal and radial indices is then investigated for the case where the strong control beam is also an OAM mode. It is shown that the conservation of OAM states is always satisfied over the OAM exchange process. Yet, an abnormal case is observed in which the radial index induces some intensity patterns of the generated beam which differs from a pure LG beam of incident beams. Analytical solutions are provided to elucidate such effects induced by radial indices on propagation characteristics of OAM beams. When superimposing two initially present weak OAM modes, it is observed that the resulting optical vortices move about the beam axis as the light propagates, forming a sort of "constellation" around the center. The shift in axis of such a composite pulse is due to the effect of interdot tunneling which is controlled by an external electric voltage. The optical angular momenta may add a new degree of freedom in the study of solid systems suitable for quantum technologies.

I. INTRODUCTION

Quantum dots (QDs) are semiconductor nanoparticles possessing wide application in quantum optics and quantum information science because of their high nonlinear optical susceptibility, large electric-dipole moments of intersubband transitions, and great flexibility in designing devices [1,2]. Their size is typically on the order of several nanometers in diameter [3]. The electrons and holes in such a scale are confined in all three spatial dimensions making artificial atoms. Closely spaced coupling of two or more quantum dots can establish a quantum-dot molecule (QDM), in which an electron can pass through the potential barrier between quantum dots via the interdot tunneling. As the QDMs cannot exhibit vibrational or rotational features, they should display somewhat different properties with respect to the usual molecules. The interdot tunneling induces the quantum coherence in QDMs which can be controlled by applying an external static gate voltage [4,5]. It is well established that quantum interference can lead to various nonlinear optical phenomena in QDMs based on the interdot tunneling. Electromagnetically induced transparency based on the interdot tunneling has been introduced in 2006 [6]. Several other works have also

studied various optical phenomena in QDMs controlled by interdot tunneling. Examples include group velocity of light pulse [7], four-wave mixing generation [8], entanglement and quantum-information transfer [9], optical bistability [10], transmission and reflection of pulse [11], and controlling the Goos-Hänchen shift [12].

On the other hand, the orbital angular momentum (OAM) of light affixes a new degree of freedom to optical technologies enabling widespread applications in data transmission, optical communication [13,14], optical tweezers [15], and quantum information [16]. The OAM light is a vortex beam which has a ring-shape intensity profile accompanied by the helical phase front [17]. Although having a history predating 1992, Allen *et al.* have been pioneers observing such twisted light beams with helical wave fronts and a phase singularity that gives rise to a dark spot in the center with no intensity [18]. Such lights with OAM can be created artificially through a variety of methods including cylindrical lens mode converters [19], spiral phase plates [20], forked diffraction gratings [21], computer-generated holograms [22], and spatial light modulators (SLMs) [23]. It is worth noting that an optical vortex, at a short wavelength, can damage the liquid-crystal-based SLMs. Moreover, the practical limitations are quite complex in the fabrication methods of the spiral phase plates for the shorter wavelength ranges of the optical vortices. Low output power and high losses are the most common drawbacks when using the mode converters and

_____

[*]mahmoudi@znu.ac.ir
[†]hamid.hamedi@tfai.vu.lt

forked diffraction gratings to generate the optical vortices with the short wavelengths. However, the nonlinear effects with the aid of quantum systems can be used to generate low loss optical twisted beams [24].

A number of interesting quantum optical effects appear when such a structured light interplays with the matter, such as the second harmonic generation (SHG) [25,26], four-wave mixing [27–30], sum-frequency generation [31], and spatially structured electromagnetically induced transparency (EIT) [32,33]. Recently and by using the Laguerre-Gaussian (LG) beams, the quantum entanglement between an ensemble of the three-level atomic systems and its spontaneous emissions has been investigated. It has been found that the atom-photon entanglement depends on the intensity profile as well as the OAM of the applied fields in the closed-loop atomic systems [34]. Besides theoretical studies, there are a number of valuable demonstrations on the interplay of matter with light carrying OAM [35–37]. The generation of an OAM-carrying ultraviolet (UV) light through SHG and OAM-entanglement frequency transducer has been experimentally examined by Zhou *et al.* [38,39]. Recent studies deal with the interaction of matter with twisted light and explore the possibility of exchange of optical vortices between different light frequencies [40–45]. The Juzeliūnas team realized the exchange of OAM modes in four- and five-level quantum systems [46,47]. The transfer of optical vortices has been shown to be possible in four-level EIT [48], coherent population trapping [49], and phaseonium media [50]. Although the exchange of optical vortices is not directly related to the topological photonics, optical vortices can be used for creating the synthetic gauge field for ultracold atoms [51,52]. Also, a vortex distortion can induce a mode associated with a topological defect in the bulk of a two-dimensional photonic material [53]. The transition from a nontrivial (vortex) to a trivial (nonvortex) state of the photon looks quite promising and may find some applications in the topological photonic area.

As is known, the transitions between different electronic states in semiconductor QD nanostructures can be optically excited by laser fields. Although plane waves have mostly been employed to study the light-matter coupling, little work has been carried out to excite QDs with the OAM light. The optical absorption of twisted light by disk-shaped semiconductor-based quantum dots have been theoretically investigated in the presence of a static magnetic field [54]. Light holes excitation by highly focused optical-vortex beams have been theoretically studied in small quantum dots [55]. Recently, the transfer of OAM of the twisted laser beam into the molecule has been investigated by calculation of induced electronic orbital currents and magnetic field [56,57].

The present work concentrates on the interaction of laser beams carrying OAM with QDMs and studies the transfer of OAM between laser fields via interdot tunneling. It is shown that due to the presence of the interdot tunneling, a single probe vortex beam initially acting on one transition of the four-level QDM generates an extra laser beam with the same vorticity as that of the incident vortex beam. Another favorable situation is then considered for the exchange of optical vortices in which the strong control beam represents also a LG beam. It is shown that the OAM number of the generated

twisted beam stays conserved during the OAM transfer. There exists an abnormal case, however, where the radial index develops some intensity-distribution patterns for the generated beam different from the initial beams. Analytical solutions are presented to explain this particular case. If the two incident beams in LG modes are initially nonzero and are superimposed, they can generate a pattern of vortices with shifted axes once the beams are propagating inside the medium. Such a composite off-axis pattern of resulting beams is due to the effect of interdot tunneling which can be controlled by an external electric voltage.

It should be noted that although both works here and in Ref. [50] utilize multilevel light-matter couplings, there exist significant differences between them. While Ref. [50] deals with nonclosed loop structures in cold atoms, here we study the light-matter propagation in QDMs with energy levels making a closed-loop level scheme. The atom-light coupling in [50] is initially prepared in a superposition of lower levels, creating a so-called phaseonium medium [58]. Moreover, the atom-light interaction is assumed to be sufficiently weak ($\Omega_i \ll \Gamma$), resulting in the transfer of vortices between weak probe fields. On the other hand, the system here is initially prepared in its ground level. In the presence of the tunneling coupling, a strong control field could excite population to an upper level. This allows the OAM of light to be transferred from the strong control field to a weak generated probe beam. Such a mechanism is completely different from the one presented in [50] as it is rather based on a sort of transparency created by the tunneling coupling (the tunneling induced transparency) [59].

Such a transfer of optical vortices may find potential application in the creation of structured light by another light [60] and in the conversion of phase information from a given input frequency to a completely different frequency. In addition, the transfer of vortices is a possible tool for the manipulation of information encoded into the OAM of light, and have implications on the inscription and storage of phase information in light-matter coupling schemes [28]. The described process allows creating a vortex at a shorter wavelength for which it is not possible to do it directly with standard optics (e.g., far infrared or UV). An optical vortex at a short wavelength can be used in high-resolution spectroscopy [61], increasing the resolution below the diffraction barrier in fluorescence microscopy [62], and entanglement of OAM states of photons [63]. It is demonstrated that the off-axis optical vortices can be used to trap and rotate both high and low index particles using the high- and low-intensity regions of the optical beam pattern, respectively [64].

The organization of the paper is as follows. In Sec. II we introduce the model and present the formulation of the basic set of equations by solving analytically the coupled Maxwell-Bloch equations. The results are presented in Sec. III, while Sec. IV summarizes the main results.

II. THEORETICAL FRAMEWORK

Let us consider a lateral quantum coupling between two self-assembled (In,Ga)As/GaAs quantum dots with different band structures. The self-assembled lateral QDMs
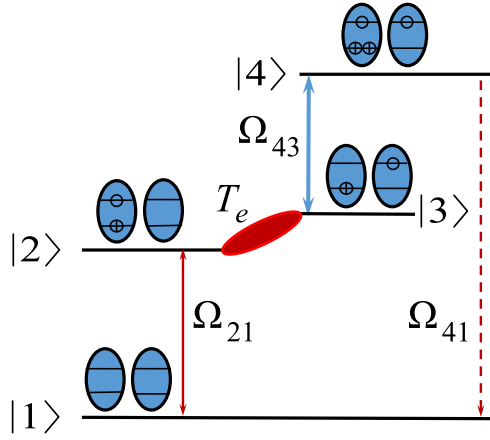
FIG. 1. Schematic band structure and level configuration of the QDM system. The electron and hole are shown by $\ominus$ and $\oplus$, respectively.

can be produced by a unique combination of molecular beam epitaxy and atomic layer precise *in situ* etching on GaAs(001) substrates which can provide a low density, about 5×10^7 cm^{-2}, homogeneous ensemble of QDMs consisting of two dots aligned along the $[1\bar{1}0]$ direction [65]. The average lateral size of each QD is almost 35 nm. The interdot barrier thickness is assumed to be a few nanometers (< 8 nm) to allow significant interdot electron tunneling to occur. The interdot coupling can be controlled by applying an external electric field along the molecular (coupling) axis via simple Schottky contacts. For further experimental details of the fabrication technique one can refer to [66].

Figure 1 illustrates a four-energy-level scheme for a double coupled QD system. The ground state defines a level in which two QDs are not excited. The state $|2\rangle$ stands for the level in which an electron is excited to the conduction band in one of the QDs to generate an exciton. The transfer of electron via interdot tunneling to the conduction band of a second QD and generation of an indirect exciton is shown by state $|3\rangle$. Finally, state $|4\rangle$ describes the biexciton which is established by exciting the electron to the conduction band of the first QD [5,67].

The transition $|i\rangle \leftrightarrow |j\rangle$ is excited by an external field with the frequency ω_{ij} and Rabi frequency $\Omega_{ij} = \vec{\mu}_{ij} \cdot \vec{E}_{ij}/\hbar (i, j \in 1, \ldots, 4)$ where μ_{ij} and E_{ij} are the induced dipole moment of the transition $|i\rangle \leftrightarrow |j\rangle$ and the amplitude of the applied field, respectively. A weak probe field is applied to the transition $|1\rangle \leftrightarrow |2\rangle$, while the transition $|3\rangle \leftrightarrow |4\rangle$ is excited by a strong control field. The states $|2\rangle$ and $|3\rangle$ are coupled by the electron tunneling process. An extra weak field with a frequency $\omega_{41} = \omega_{21} + \omega_{32} + \omega_{43}$ is generated due to the three-wave mixing. Note that ω_{32} is considered to be zero owing to the negligible energy difference of the transition $|2\rangle \leftrightarrow |3\rangle$.

It is assumed that each pair of QDs is placed at a distance much smaller than the relevant wavelength of applied fields and the spatial dependence of the applied fields is dropped (the dipole approximation), leading to the elimination of the magnetic component of applied fields.

Applying the dipole and rotating-wave approximations, the interaction Hamiltonian of the system can be written as

$$H = \sum_j \varepsilon_j |j\rangle\langle j| + T_e(|2\rangle\langle 3| + |3\rangle\langle 2|)$$
$$- \hbar[\Omega_{21}^* e^{i\Delta_{21}t}|1\rangle\langle 2| + \Omega_{43} e^{-i\Delta_{43}t}|4\rangle\langle 3|$$
$$+ \Omega_4^* e^{i\Delta_{41}t}|1\rangle\langle 4| + \text{H.c.}], \tag{1}$$

where ε_j is the energy of the state $|j\rangle$ and $\Delta_{ij} = \omega_{ij} - \overline{\omega}_{ij}$ describes the frequency detuning between the applied laser field and resonant frequency, associating with the corresponding transitions, $|i\rangle \leftrightarrow |j\rangle$. The parameter T_e represents the strength of the interdot tunneling between the states $|2\rangle$ and $|3\rangle$ created by a static electric field. The density-matrix equations for the matter fields are

$$\dot{\rho}_{11} = 2\Gamma_{21}\rho_{22} + 2\Gamma_{41}\rho_{44} + i\Omega_{21}^*\rho_{21} - i\Omega_{21}\rho_{12} + i\Omega_{41}^*\rho_{41}$$
$$- i\Omega_{41}\rho_{14},$$
$$\dot{\rho}_{22} = -2\Gamma_{21}\rho_{22} + i\Omega_{21}\rho_{12} - i\Omega_{21}^*\rho_{21} + iT_e(\rho_{32} - \rho_{23}),$$
$$\dot{\rho}_{33} = 2\Gamma_{43}\rho_{44} + i\Omega_{43}^*\rho_{43} - i\Omega_{43}\rho_{34} + iT_e(\rho_{23} - \rho_{32}),$$
$$\dot{\rho}_{12} = -(i\Delta_{21} + \Gamma_{21})\rho_{12} + i\Omega_{21}(\rho_{22} - \rho_{11}) - iT_e\rho_{13}$$
$$+ i\Omega_{41}^*\rho_{42},$$
$$\dot{\rho}_{13} = -i[\Delta_{41} - \Delta_{43}]\rho_{13} - i\Omega_{43}\rho_{14} + i\Omega_{21}^*\rho_{23} + i\Omega_{41}^*\rho_{43}$$
$$- iT_e\rho_{12},$$
$$\dot{\rho}_{14} = -[i\Delta_{41} + \Gamma_{41}]\rho_{14} - i\Omega_{43}^*\rho_{13} + i\Omega_{41}(\rho_{44} - \rho_{11})$$
$$+ i\Omega_{21}^*\rho_{24},$$
$$\dot{\rho}_{23} = -\Gamma_{21}\rho_{23} - i[\Delta_{41} - \Delta_{21} - \Delta_{43}]\rho_{23} + i\Omega_{21}\rho_{13}$$
$$- i\Omega_{43}\rho_{24} + iT_e(\rho_{33} - \rho_{22}),$$
$$\dot{\rho}_{24} = -[(i(\Delta_{41} - \Delta_{21}) + \Gamma_{21} + \Gamma_{43} + \Gamma_{41})]\rho_{24} + iT_e\rho_{34}$$
$$+ i\Omega_{21}\rho_{14} - i\Omega_{43}^*\rho_{23} - i\Omega_{41}^*\rho_{21},$$
$$\dot{\rho}_{34} = -[i\Delta_{43} + (\Gamma_{41} + \Gamma_{43})]\rho_{34} + iT_e\rho_{24} - i\Omega_{41}^*\rho_{31}$$
$$+ i\Omega_{43}^*(\rho_{44} - \rho_{33}),$$
$$\dot{\rho}_{44} = -(\dot{\rho}_{11} + \dot{\rho}_{22} + \dot{\rho}_{33}). \tag{2}$$

The above density-matrix equations represent the evolution of the system affected by the laser fields and tunneling coupling. They follow from the general quantum Liouville equation for the density-matrix operator

$$\frac{\partial \rho}{\partial t} = \frac{-i}{\hbar}[H, \rho] + L(\rho), \tag{3}$$

where the damping operator $L(\rho)$ describes the decoherence processes. The steady-state analytical expressions for the coherence terms ρ_{21} and ρ_{41} can be obtained, by solving Eq. (2) for $\Gamma_{21} = \Gamma_{41} = \Gamma_{43} = \gamma$ under multiphoton resonance condition, $\Delta_{43} = 0$, $\Delta_{21} = \Delta_{41} = \Delta$, giving

$$\rho_{21} = \frac{(T_e\Omega_{41} - \Omega_{43}\Omega_{21})\Omega_{43}^* + i(\gamma\Delta - \Delta^2)\Omega_{21}}{(\gamma - i\Delta)(iT_e^2 + \gamma\Delta - i\Delta^2 + i|\Omega_{43}|^2)},$$

$$\rho_{41} = -\frac{T_e(T_e\Omega_{41} - \Omega_{43}\Omega_{21}) - i\gamma\Delta\Omega_{41} - \Delta^2\Omega_{41}}{(\gamma - i\Delta)(iT_e^2 + \gamma\Delta - i\Delta^2 + i|\Omega_{43}|^2)}. \tag{4}$$

The Maxwell wave equations in the slowly varying envelope approximation read

$$\frac{\partial \Omega_{21}(z)}{\partial z} = i \frac{\alpha \gamma}{2L} \rho_{21},$$

$$\frac{\partial \Omega_{41}(z)}{\partial z} = i \frac{\alpha \gamma}{2L} \rho_{41}, \tag{5}$$

where L and α are the length of the QDM ensemble and the optical depth for both fields [48], respectively. Substituting Eq. (4) into Eq. (5) and assuming $\Delta = 0$, $\Omega_{41}(z = 0) = 0$, and $\Omega_{21}(z = 0) = \Omega_{21}$, one arrives at the following equations:

$$\Omega_{21}(r, \varphi, z) = \frac{\Omega_{21}(r, \varphi)\left[T_e^2 + \exp\left(-\frac{z\alpha}{2L}\right)|\Omega_{43}|^2\right]}{T_e^2 + |\Omega_{43}|^2} \tag{6}$$

and

$$\Omega_{41}(r, \varphi, z) = -\frac{\left[-1 + \exp\left(-\frac{z\alpha}{2L}\right)\right]T_e\Omega_{21}(r, \varphi)\Omega_{43}}{T_e^2 + |\Omega_{43}|^2}, \tag{7}$$

which describe the propagation of fields inside the medium.

III. RESULTS AND DISCUSSIONS

The complex form describing the distribution of the field amplitude of a LG beam can be expressed cylindrically as

$$\Omega(r, \varphi) = \Omega_0 \frac{1}{\sqrt{|l|!}} \left(\frac{\sqrt{2}r}{w_{LG}}\right)^{|l|} L_p^{|l|}\left(2r^2/w_{LG}^2\right)e^{-r^2/w_{LG}^2}e^{il\varphi}, \tag{8}$$

where Ω_0, w_{LG}, l, and p show the constant Rabi frequency, beam waist radius, and azimuthal (OAM) and radial indices of the LG modes, respectively. Here, the associated Laguerre polynomial, $L_p^{|l|}$, has the form

$$L_p^{|l|}(x) = \frac{e^x x^{-|l|}}{p!} \frac{d^p}{dx^p}[x^{|l|+p}e^{-x}], \tag{9}$$

with $x = 2r^2/w_{LG}^2$ determining the radial dependence of the LG beams for different radial mode numbers. When l is not zero, the LG light beams possess OAM along the optical axis.

A. Exchange of vortices

Let us now consider the spatial profile of the laser fields described by Eq. (8). As Eq. (7) shows, the Rabi frequency of the generated third field corresponds to the interdot tunneling as well as the Rabi frequency of the probe and the strong control fields. Thus, the generated laser field Ω_{41} is a vortex if any of the fields Ω_{21}, Ω_{43}, or both of them are initially vortices. Such a transfer of optical vortices is because of the presence of the interdot tunneling which can be controlled by applying an external electric voltage. Let us first assume that only the probe field Ω_{21} is vortex. The effect of the interdot tunneling strength, T_e, on the dimensionless intensity of the generated field $|\Omega_{41}(z)|^2/|\Omega_{21}(0)|^2$ has been shown by means of Eq. (7). The dimensionless plot for the intensity of the generated OAM field as a function of the tunneling strength is shown at $z = L$ in Fig. 2 for $w_{LG} = 0.5$ mm, $\Omega_{43} = \gamma$, and $\alpha = 20$. As expected, the intensity of the generated third field is zero when the interdot tunneling strength is zero, $T_e = 0$. The generated third field grabs its maximal value for $T_e = 1$.
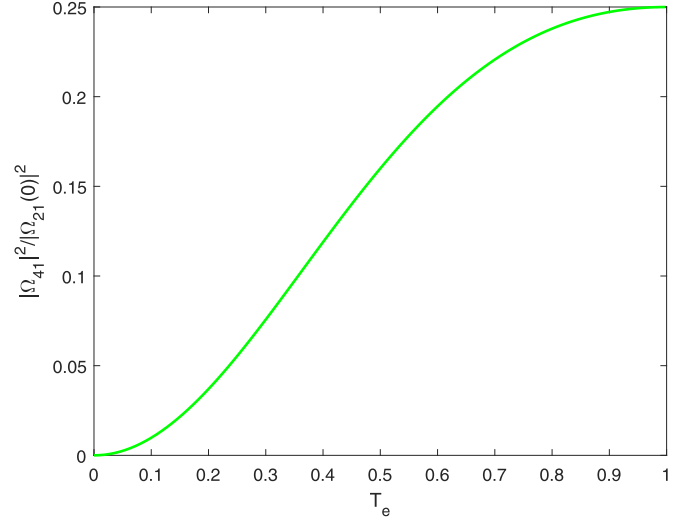

FIG. 2. The dimensionless intensity of the generated third field $|\Omega_{41}(z)|^2/|\Omega_{21}(0)|^2$ versus the tunneling strength for $z = L$, $\Omega_{43} = \gamma$, and $\alpha = 20$.

This is an optimal value of tunneling coupling for which the intensity of the generated OAM mode is the largest.

Next we consider the optimal interdot tunneling effect and investigate the intensity of the probe and generated third beams inside the QDM medium, using Eqs. (6) and (7). Figure 3 shows the dimensionless intensities $|\Omega_{21}(z)|^2/|\Omega_{21}(0)|^2$ and $|\Omega_{41}(z)|^2/|\Omega_{21}(0)|^2$ against the dimensionless distance z/L for $T_e = 1$. The other parameters are the same as in Fig. 2. One can see that the laser field Ω_{41} has not yet been created at the beginning of the ensemble where the weak probe beam has just entered. Propagating inside the QD ensemble, the beam Ω_{41} is generated. Equations (6) and (7) and Fig. 3 indicate that both OAM beams experience energy losses mostly at the beginning of the ensemble; going deeper into the ensemble, losses disappear where the system is transferred to some transparency state (see Fig. 3).
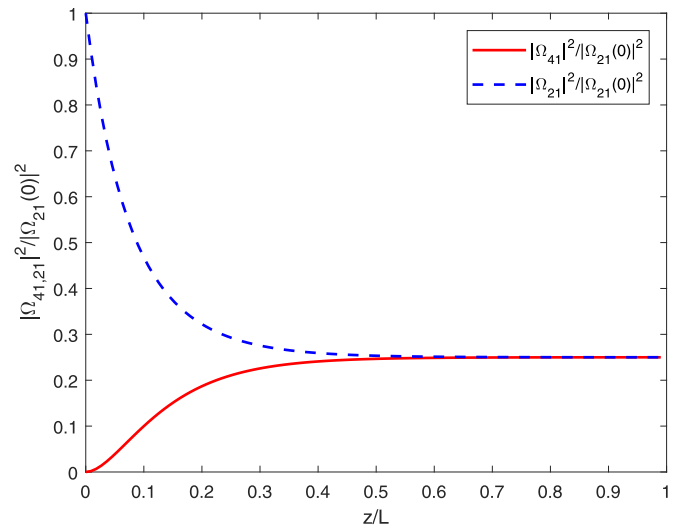

FIG. 3. The dimensionless intensity of fields $|\Omega_{21}(z)|^2/|\Omega_{21}(0)|^2$ and $|\Omega_{41}(z)|^2/|\Omega_{21}(0)|^2$ versus the dimensionless distance z/L for $T_e = 1$. Other parameters are the same as in Fig. 2.
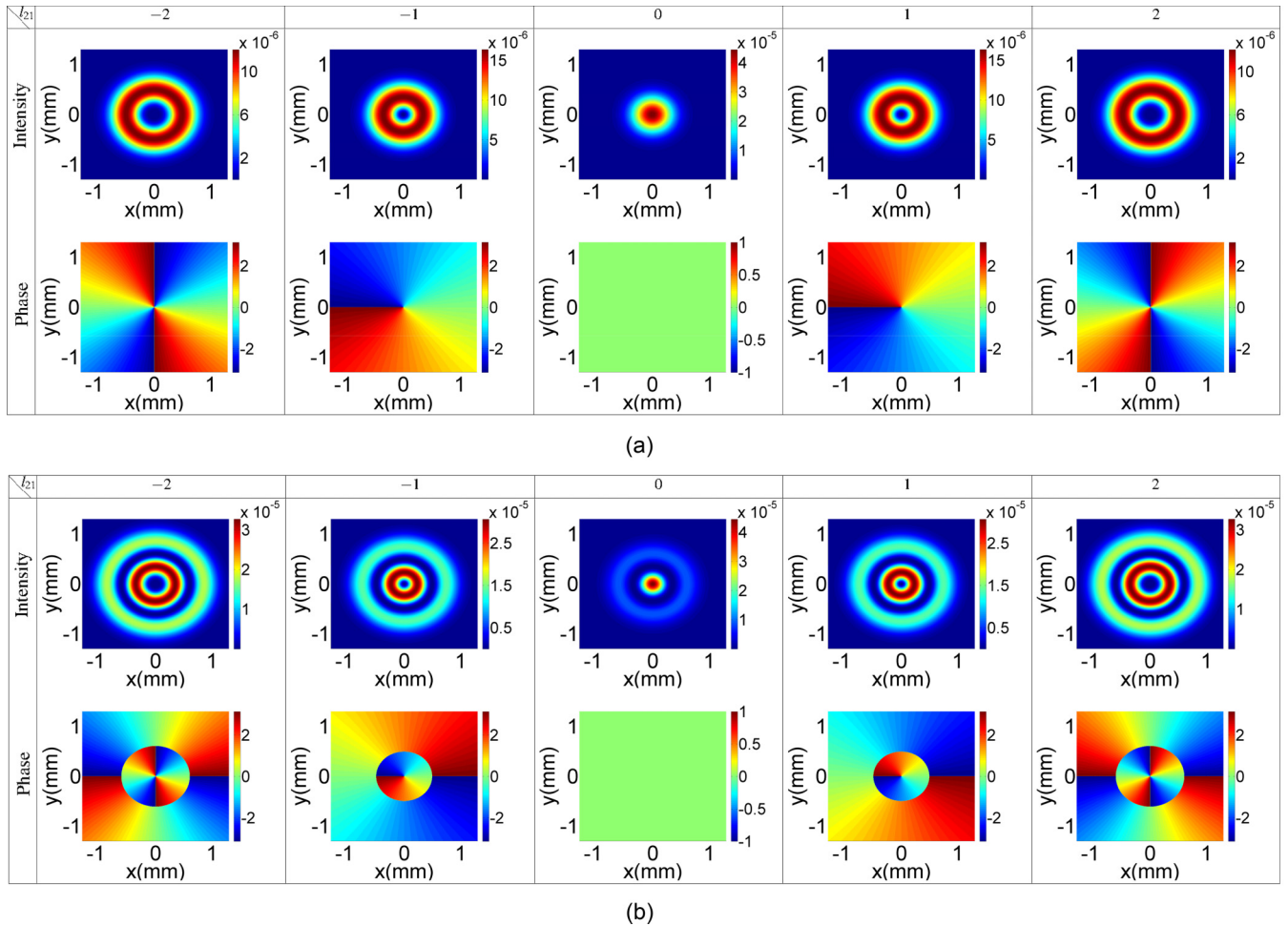
(a)

(b)

FIG. 4. The intensity and phase profiles of the generated third field as a function of x and y for the different modes of the probe LG field, $l_{21} = -2, -1, \ldots, 2$, with $p_{21} = 0$ (a) and $p_{21} = 1$ (b). The interdot tunneling parameter, beam waist, and constant Rabi frequency of the probe LG field are chosen as $T_e = 1$, $w_{LG} = 0.5$ mm, and $\Omega_{21_0} = 0.01\gamma$, respectively. The value of the interdot tunneling parameter is $T_e = 1$. Other parameters are the same as in Fig. 2.

In what follows, we proceed with the numerical simulations to describe such a swapping in OAM modes based on the interdot tunneling effect.

1. First case: Only Ω_{21} is a vortex

In Fig. 4(a), we show the intensity and phase profiles of the generated OAM mode as a function of x and y for different winding numbers $l_{21} = -2, -1, \ldots, 2$ but with zero radial index $p_{21} = 0$. The horizontal and vertical axes x and y are scaled in millimeters. We take $T_e = 1$, $w_{LG} = 0.5$ mm, and $\Omega_{21_0} = 0.01\gamma$, and the other parameters the same as in Fig. 2. It is observed that the intensity profile of the third generated field has a Gaussian profile when $l_{21} = 0$. Yet, the doughnut intensity profiles appear with a dark (blue) hollow center for nonzero l_{21}, indicating a conserved transfer of optical vortex of the probe beam to the generated third beam. The diameter of the doughnuts increases for the larger topological charges l_{21}. The helical phase patterns help to realize the nature of the singularity at the core of the generated third OAM beam. No singularity takes place at phase patterns when $l_{21} = 0$, confirming a Gaussian-shaped wave front of the laser field

with a normal phase. The phase patterns start twisting for nonzero vorticities.

Note that all profiles shown in Fig. 4(a) exhibit a single ring in their intensity patterns, indicating their radial indices are all at zero. Let us study in Fig. 4(b), the effect of the nonzero radial index p ($p_{21} = 1$) on the intensity and phase profiles of the generated OAM field for the different azimuthal indices $l_{21} = -2, -1, \ldots, 2$. While the central dark holes always exist for nonzero vorticities, the radial index of the probe LG beam develops some remarkable changes in the intensity and phase profiles of the generated third field. In particular, there exists now a dark ring between two bright rings in each diagram for the intensity profile. However, measuring an intensity profile is not always a very accurate way to determine different mode indices for a particular vortex beam, as sometimes the bright rings are too dim to be distinguished by the naked eye (e.g., see intensity diagrams shown later in Fig. 5). Helical phase profiles, instead, provide an accurate and convenient way to check for different azimuthal and radial indices. As an example, let us read the case with $l_{21} = 2$ and $p_{21} = 1$, illustrated in the last diagram in the second row of Fig. 4(b). The phase jumps from 0 to $2 \times 2\pi = 4\pi$ at the
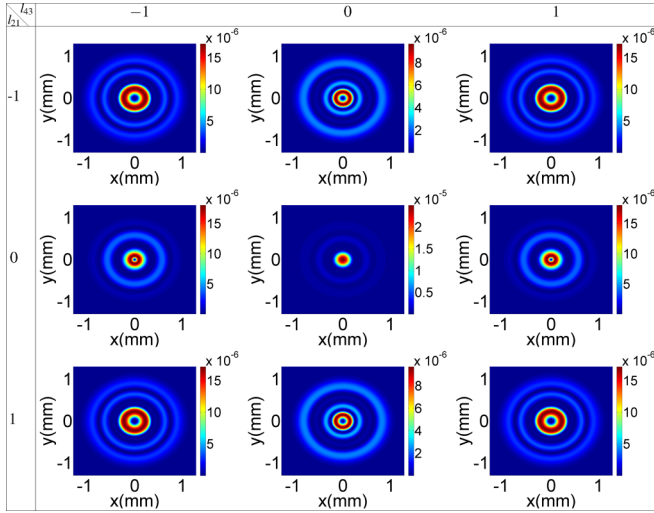
FIG. 5. The intensity profiles of the generated field versus x and y for different modes of the weak probe and strong control LG fields with $p_{21} = 1$, $p_{43} = 2$, $l_{21}, l_{43} \in -1, 0, 1$, $\Omega_{21_0} = 0.01\gamma$, and $\Omega_{43_0} = \gamma$. Other parameters are the same as in Fig. 4.
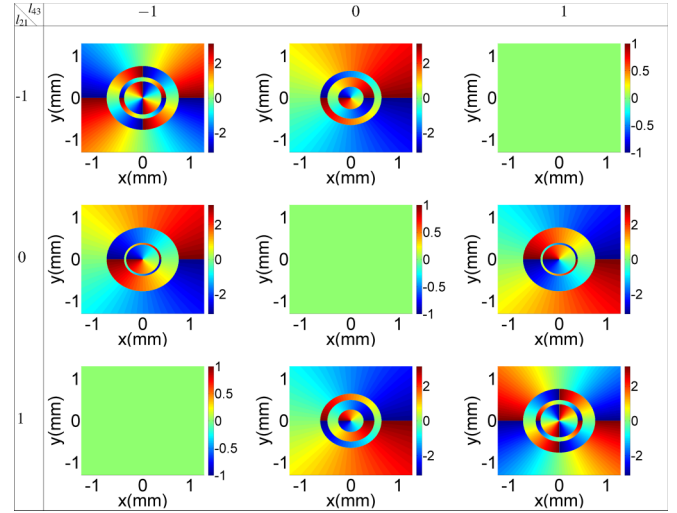

FIG. 6. The phase profiles of the generated third field versus x and y for the different modes of the applied LG fields. The parameters used here are the same as in Fig. 5.

beam center, indicating an azimuthal index l_{21} equal to 2. Two zones appear from the core to the border of the phase profile; at their boundary the phase diagram experiences a π shift, where the corresponding light goes to zero in intensity. The radial index for the generated beam is read to be 1, which is due to the existence of two zones in the profile separated by one π-shift boundary circle. To read and identify l and p numbers for any unknown vortex beam, one can develop a general manner; the azimuthal index is read with nl if the phase jumps from 0 to $2n\pi$ around the singularity point, while the radial index is read with mp if the phase diagram demonstrates a number of $m\pi$-shift boundary circles from the radial direction. One can use the above manner to distinguish different azimuthal and radial indices for more complex vortex beams such as those described in the next sections.

2. Second case: Both Ω_{21} and Ω_{43} are vortices

Next, we study a situation where both Ω_{21} and Ω_{43} describe optical vortices. In Fig. 5, we depict the intensity of the generated third field as a function of x and y for different modes of the probe and strong control LG beams with $p_{21} = 1$, $p_{43} = 2$, $l_{21}, l_{43} \in -1, 0, 1$, $\Omega_{21_0} = 0.01\gamma$, and $\Omega_{43_0} = \gamma$, while the other parameters are the same as in Fig. 4. Figure 6 shows the corresponding phase patterns.

It is seen that the generated third beam develops a new OAM state with the total azimuthal index of $l_{21} + l_{43}$, meaning that the total azimuthal index of applied beams remains constant over the OAM exchange process. This is quite understandable from Eq. (7) as it is as a result of the OAM conservation. In a particular case when $l_{21} = -l_{43} \neq 0$, the generated third beam is no longer a vortex as the total topological charge associated with the sum of incident beams becomes zero. As an example, let us consider the last diagrams in the first row in Figs. 5 and 6. As expected, the phase diagram of the generated beam shows no singularity at the core. However,

the intensity profile demonstrates a multiring pattern. Note that such a pattern is not called a vortex, although it has a zero intensity at the beam center. This abnormal intensity distribution is due to the nonzero radial index for the incident beams Ω_{21} and Ω_{43}. According to Eqs. (8) and (9), the radial coordinate dependence of the LG beam is modified when $p > 0$, resulting in $p + 1$ concentric rings in the intensity profiles with zero-intensity center.

According to Eq. (7), the generated third field is proportional to the product of the weak probe Ω_{21} and strong control Ω_{43} fields which are considered as the LG modes. When $p = 0$, the product of two Rabi frequencies of the LG modes makes a single mode with $l = l_{21} + l_{41}$, but the situation is completely different for $p > 0$. The product of two LG modes can be expanded as a linear superposition of different LG modes. The appropriate superposition of the contributing LG modes of the generated third field has been analytically obtained for several different LG modes. The detail of calculation is given in the Appendix when $l_{21} = -1$, $p_{21} = 1$ and $l_{41} = -1$, $p_{41} = 2$. The coefficients appearing in the superposition mode determine the contribution of each LG mode to generate the third field. The intensity and phase profiles of the corresponding linear superpositions are shown in Fig. 7 for several different LG modes. The first and second rows show the characteristics of the weak probe and strong control fields, respectively, while the third row illustrates the linear superposition for different LG modes forming the generated third field. Note that such a linear superposition state of different LG modes takes place only under the effect of the QDM medium. Therefore, the transfer of OAMs is accompanied by the exchange of different radial modes of the applied LG fields.

B. Composite vortices

Let us next consider a case where both vortex beams $\Omega_{41}(z = 0) = \Omega_{41}(r, \varphi)$ and $\Omega_{21}(z = 0) = \Omega_{21}(r, \varphi)$ are incident on the medium. The analytical expression describing the

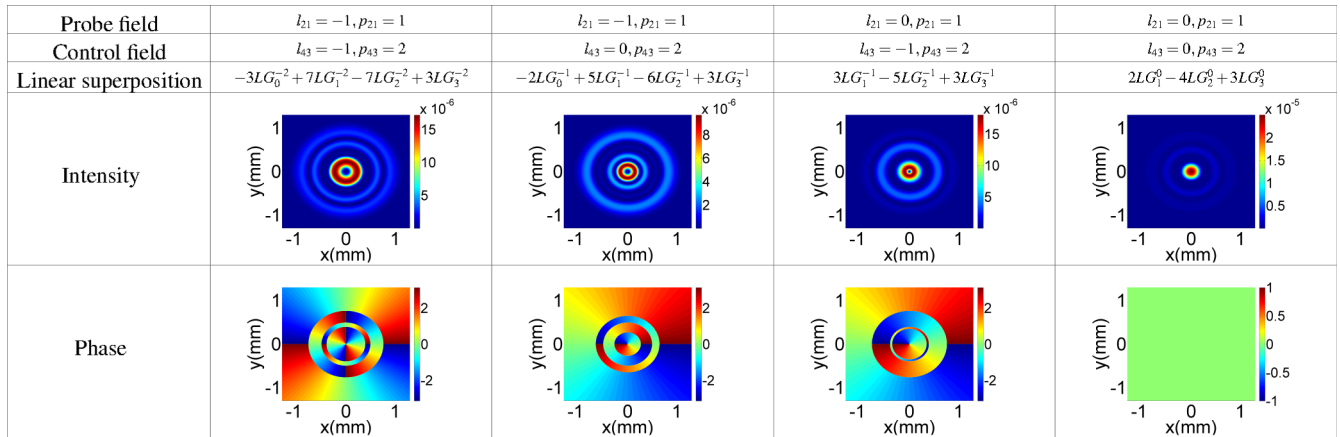| Probe field	$l_{21}=-1, p_{21}=1$	$l_{21}=-1, p_{21}=1$	$l_{21}=0, p_{21}=1$	$l_{21}=0, p_{21}=1$
Control field	$l_{43}=-1, p_{43}=2$	$l_{43}=0, p_{43}=2$	$l_{43}=-1, p_{43}=2$	$l_{43}=0, p_{43}=2$
Linear superposition	$-3LG_0^{-2}+7LG_1^{-2}-7LG_2^{-2}+3LG_3^{-2}$	$-2LG_0^{-1}+5LG_1^{-1}-6LG_2^{-1}+3LG_3^{-1}$	$3LG_1^{-1}-5LG_2^{-1}+3LG_3^{-1}$	$2LG_1^0-4LG_2^0+3LG_3^0$
Intensity				
Phase				

FIG. 7. The intensity and phase profiles of the corresponding superposition states by considering the effect of the QDM medium.

propagation of Ω_{41} then takes the form

$$\Omega_{41}(r,\varphi,z) = \frac{\left[\exp\left(-\frac{z\alpha}{2L}\right)T_e^2+|\Omega_{43}|^2\right]\Omega_{41}(r,\varphi)}{T_e^2+|\Omega_{43}|^2}$$
$$+ \frac{\left[1-\exp\left(-\frac{z\alpha}{2L}\right)\right]T_e\Omega_{43}\Omega_{21}(r,\varphi)}{T_e^2+|\Omega_{43}|^2}. \quad (10)$$

The intensity and helical phase profiles of the generated field Ω_{41} are displayed in Figs. 8 and 9 for different interdot tunneling parameters, $T_e = 0$, 0.5, and 1. Different modes of the probe LG fields are considered, i.e., ($l_{21}=1, l_{41}=2$), ($l_{21}=1, l_{41}=3$), ($l_{21}=1, l_{41}=4$), and ($l_{21}=1, l_{41}=5$), while $p_{21}=p_{41}=0$. We take $\Omega_{41_0}=0.01\gamma$ and the other

parameters are the same as in Fig. 2. The left column of Fig. 8 shows that for $T_e = 0$, the two incident LG fields, $\Omega_{41}(0)$ and $\Omega_{21}(0)$, do not interact with each other; hence, the output field featured by Eq. (10) contains the same vorticity as the input field $\Omega_{41}(0)$. The incident applied LG fields start interacting in the presence of the interdot tunneling effect, forming the composite vortices. The tunneling coupling grows more singularities at the transverse plane associated with zero-intensity regions. For instance, when $T_e = 0.5$ (as indicated in the middle columns), the resulting composite beam Ω_{41} exhibits a singularity at the core surrounded by some peripheral vortices (constellation patterns). Increasing the interdot tunneling parameter to $T_e = 1$, moves the position of peripheral vortices far away from the central vortex. Generally speaking, if $|l_{21}| < |l_{41}|$, the resulting composite beam acquires a vortex of vorticity $|l_{21}|$ located at the beam core which is surrounded by $|l_{21}-l_{41}|$ peripheral vortices.

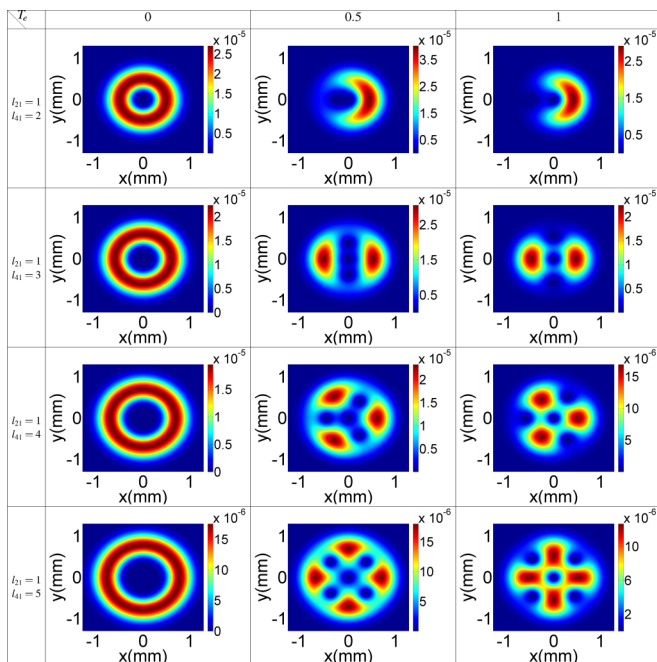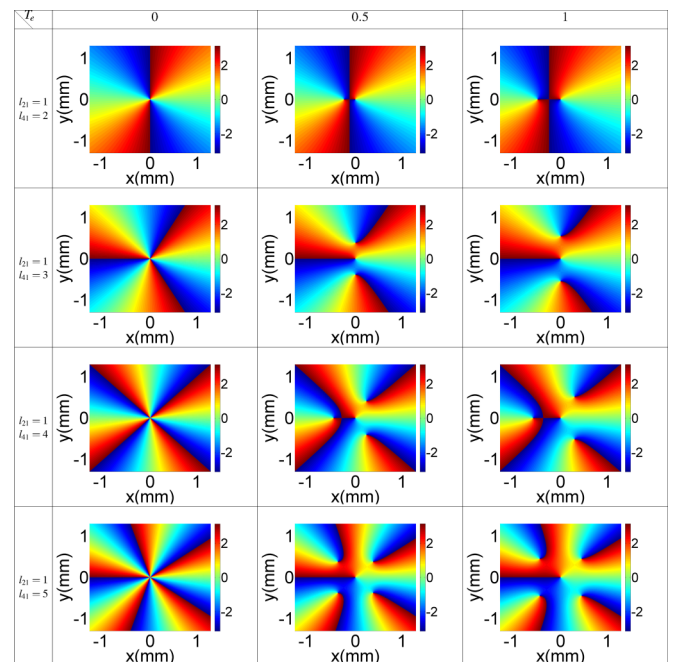FIG. 8. The intensity profiles of the third field versus x and y for the different modes of the probe LG fields, i.e., ($l_{21}=1, l_{41}=2$), ($l_{21}=1, l_{41}=3$), ($l_{21}=1, l_{41}=4$), and ($l_{21}=1, l_{41}=5$), with $p_{21}=p_{41}=0$ for different interdot tunneling parameters, $T_e = 0$, 0.5, and 1. The constant Rabi frequency of the third field is chosen as $\Omega_{41_0}=0.01\gamma$ and the other parameters are the same as in Fig. 2.

FIG. 9. The phase profiles of the third field versus x and y. The parameters used here are the same as in Fig. 8.

IV. CONCLUDING REMARKS

To conclude, we have investigated the interplay of light beams with OAM with structural asymmetry quantum-dot molecules with four energy levels. It has been shown that the interdot tunneling effect can induce the OAM transfer between different frequencies. We have considered a particular situation where a weak probe beam is initially a vortex beam. Due to the effect of tunneling coupling, an extra laser is generated with the same winding number as that of the incident probe field. An efficient condition is considered for such exchange of optical vortices. We have also studied the propagation of LG beams with azimuthal and radial indices when the strong control beam is also an OAM mode. An abnormal case is observed in which the radial index induces some intensity patterns for the generated beam which is quite different from the incident pure LG beams. An analytical model is presented to understand such an effect of radial index. We have also shown that when the two vortex beams are present at the beginning of the medium and as a result of tunneling coupling, composite vortices can take place with shifted axes.

APPENDIX

In this Appendix, we evaluate the pure LG modes that contributed to the generation of the third field. Considering two applied fields as

$$\Omega_{21}(r,\varphi) = \Omega_{21_0} \frac{1}{\sqrt{|l_{21}|!}} \left(\frac{\sqrt{2}r}{w_{\text{LG}}}\right)^{|l_{21}|} e^{-il_{21}\varphi}$$
$$\times L_1^{|l_{21}|}\left(2r^2/w_{LG}^2\right) e^{-r^2/w_{\text{LG}}^2},$$

$$\Omega_{43}(r,\varphi) = \Omega_{43_0} \frac{1}{\sqrt{|l_{43}|!}} \left(\frac{\sqrt{2}r}{w_{\text{LG}}}\right)^{|l_{43}|} e^{-il_{43}\varphi}$$
$$\times L_2^{|l_{43}|}\left(2r^2/w_{\text{LG}}^2\right) e^{-r^2/w_{\text{LG}}^2}, \tag{A1}$$

with $l_{21} = l_{43} = -1$, the generated third field has the form

$$\Omega_{41}(r,\varphi,z) = -\frac{\left[-1 + \exp\left(-\frac{z\alpha}{2L}\right)\right] T_e \Omega_{21} \Omega_{43}}{T_e^2 + |\Omega_{43}|^2}$$
$$= -\frac{\left[-1 + \exp\left(-\frac{z\alpha}{2L}\right)\right] T_e}{T_e^2 + |\Omega_{43}|^2} \Omega_{21_0} \Omega_{43_0}$$
$$\times \left(\frac{1}{\sqrt{|-1|!}}\right)^2 \left[\left(\frac{\sqrt{2}r}{w_{LG}}\right)^{|-1|}\right]^2$$
$$\times e^{-2r^2/w_{\text{LG}}^2} e^{-2i\varphi} L_1^{|-1|}\left(2r^2/w_{\text{LG}}^2\right)$$
$$\times L_2^{|-1|}\left(2r^2/w_{\text{LG}}^2\right). \tag{A2}$$

Some of the associated Laguerre polynomials can be used for obtaining the superposition of the pure LG modes forming the generated third field. The needed associated Laguerre polynomials are

$$L_1^{|-1|}(x) = (2 - x),$$
$$L_2^{|-1|}(x) = \tfrac{1}{2}(6 - 6x + x^2),$$
$$L_0^{|-2|}(x) = 1,$$
$$L_1^{|-2|}(x) = 3 - x,$$
$$L_2^{|-2|}(x) = \tfrac{1}{2}(12 - 8x + x^2),$$
$$L_3^{|-2|}(x) = \tfrac{1}{6}(60 - 60x + 15x^2 - x^3). \tag{A3}$$

Substituting Eq. (A3) into Eq. (A2), the following superposition of pure LG modes is obtained for the generated third field

$$\Omega_{41}(r,\varphi,z) = -\frac{\left[-1 + \exp\left(-\frac{z\alpha}{2L}\right)\right] T_e}{T_e^2 + |\Omega_{43}|^2} \Omega_{21_0} \Omega_{43_0} \left(\frac{1}{\sqrt{|-1|!}}\right)^2 \left[\left(\frac{\sqrt{2}r}{w_{\text{LG}}}\right)^{|-1|}\right]^2 e^{-2r^2/w_{\text{LG}}^2} e^{-2i\varphi} \left(6 - 9x + 4x^2 - \frac{1}{2}x^3\right),$$

$$= -\frac{\left[-1 + \exp\left(-\frac{z\alpha}{2L}\right)\right] T_e}{T_e^2 + |\Omega_{43}|^2} \Omega_{21_0} \Omega_{43_0} e^{-r^2/w_{\text{LG}}^2} \left(-3\text{LG}_0^{-2} + 7\text{LG}_1^{-2} - 7\text{LG}_2^{-2} + 3\text{LG}_3^{-2}\right), \tag{A4}$$

in which LG_p^l indicates a pure LG mode with the radial index p and azimuthal index l.

[1] H. Oosterkamp, T. Fujisawa, W. G. Van Der Wiel, K. Ishibashi, R. V. Hijman, and S. Tarucha, Nature (London) **395**, 873 (1998).

[2] A. Zrenner, E. Beham, S. Stufler, F. Findeis, M. Bichler, and G. Abstreiter, Nature (London) **418**, 612 (2002).

[3] R. C. Ashoori, Nature (London) **379**, 413 (1996).

[4] J. M. Villas-Bôas, A. O. Govorov, and S. E. Ulloa, Phys. Rev. B **69**, 125342 (2004).

[5] K. Müller, A. Bechtold, C. Ruppert, M. Zecherle, G. Reithmaier, M. Bichler, H. J. Krenner, G. Abstreiter, A. W. Holleitner, J. M. Villas-Bôas, M. Betz, and J. J. Finley, Phys. Rev. Lett. **108**, 197402 (2012).

[6] C. H. Yuan and K. D. Zhu, Appl. Phys. Lett. **89**, 052115 (2006).

[7] M. Mahmoudi and M. Sahrai, Physica E **41**, 1772 (2009).

[8] A. Sitek and P. Machnikowski, Phys. Status Solidi C **6**, 492 (2009).

[9] X. Y. Lü, J. Wu, L. L. Zheng, and Z. M. Zhan, Phys. Rev. A **83**, 042302 (2011).

[10] A. Vafafard, S. Goharshenasan, N. Nozari, A. Mortezapour, and M. Mahmoudi, J. Lumin. **134**, 900 (2013).

[11] R. Nasehi, M. Mahmoudi, and M. Sahrai, Laser Phys. **26**, 115202 (2016).

[12] R. Nasehi, S. H. Asadpour, H. Rahimpour Soleimani, and M. Mahmoudi, Chin. Phys. Lett. **33**, 014204 (2016).

[13] J. Wang, J. Y. Yang, I. M. Fazal, N. Ahmed, Y. Yan, H. Huang, Y. Ren, Y. Yue, S. Dolinar, M. Tur, and A. E. Willner, Nat. Photonics **6**, 488 (2012).

[14] N. Bozinovic, Y. Yue, Y. Ren, M. Tur, P. Kristensen, H. Huang, A. E. Willner, and S. Ramachandran, Science **340**, 1545 (2013).

[15] M. Padgett and R. Bowman, Nat. Photonics **5**, 343 (2011).

[16] G. Molina-Terriza, J. P. Torres, and L. Torner, Nat. Phys. **3**, 305 (2007).

[17] *The Angular Momentum of Light*, edited by D. L. Andrews and M. Babiker (Cambridge University Press, Cambridge, UK, 2012).

[18] L. Allen, M. W. Beijersbergen, R. J. C. Spreeuw, and J. P. Woerdman, Phys. Rev. A **45**, 8185 (1992).

[19] M. W. Beijersbergen, L. Allen, H. E. L. O. Van der Veen, and J. P. Woerdman, Opt. Commun. **96**, 123 (1993).

[20] M. W. Beijersbergen, R. P. C. Coerwinkel, M. Kristensen, and J. P. Woerdman, Opt. Commun. **112**, 321 (1994).

[21] V. Yu. Bazhenov, M. V. Vasnetsov, and M. S. Soskin, Pis'ma Zh. Eksp. Teor. Fiz. **52**, 1037 (1990) [JETP Lett. **52**, 429 (1990)].

[22] N. R. Heckenberg, R. McDuff, C. P. Smith, and A. G. White, Opt. Lett. **17**, 221 (1992).

[23] A. Jesacher, A. Schwaighofer, S. Fürhapter, C. Maurer, S. Bernet, and M. Ritsch-Marte, Opt. Express **15**, 5801 (2007).

[24] N. A. Chaitanya, S. C. Kumar, K. Devi, G. K. Samanta, and M. Ebrahim-Zadeh, Opt. Lett. **41**, 2715 (2016).

[25] K. Dholakia, N. B. Simpson, M. J. Padgett, and L. Allen, Phys. Rev. A **54**, R3742 (1996).

[26] J. Courtial, K. Dholakia, L. Allen, and M. J. Padgett, Phys. Rev. A **56**, 4193 (1997).

[27] S. Barreiro, J. W. R. Tabosa, J. P. Torres, Y. Deyanova, and L. Torner, Opt. Lett. **29**, 1515 (2004).

[28] G. Walker, A. S. Arnold, and S. Franke-Arnold, Phys. Rev. Lett. **108**, 243601 (2012).

[29] D. Persuy, M. Ziegler, O. Crégut, K. Kheng, M. Gallart, B. Hönerlage, and P. Gilliot, Phys. Rev. B **92**, 115312 (2015).

[30] R. N. Lanning, Z. Xiao, M. Zhang, I. Novikova, E. E. Mikhailov, and J. P. Dowling, Phys. Rev. A **96**, 013830 (2017).

[31] Y. Li, Z. Y. Zhou, D. S. Ding, and B. S. Shi, J. Opt. Soc. Am. B **32**, 407 (2015).

[32] N. Radwell, T. W. Clark, B. Piccirillo, S. M. Barnett, and S. Franke-Arnold, Phys. Rev. Lett. **114**, 123603 (2015).

[33] H. R. Hamedi, V. Kudriašov, J. Ruseckas, and G. Juzeliūnas, Opt. Express **26**, 28249 (2018).

[34] Z. Amini Sabegh, R. Amiri, and M. Mahmoudi, Sci. Rep. **8**, 13840 (2018).

[35] N. B. Clayburn, J. L. McCarter, J. M. Dreiling, M. Poelker, D. M. Ryan, and T. J. Gay, Phys. Rev. B **87**, 035204 (2013).

[36] M. A. Noyan and J. M. Kikkawa, Appl. Phys. Lett. **107**, 032406 (2015).

[37] K. Shigematsu, K. Yamane, R. Morita, and Y. Toda, Phys. Rev. B **93**, 045205 (2016).

[38] Z. Y. Zhou, D. S. Ding, Y. K. Jiang, Y. Li, S. Shi, X. S. Wang, and B. S. Shi, Opt. Express **22**, 20298 (2014).

[39] Z. Y. Zhou, Y. Li, D. S. Ding, W. Zhang, S. Shi, B. S. Shi, and G. C. Guo, Light: Sci. Appl. **5**, e16019 (2016).

[40] H. R. Hamedi, J. Ruseckas, E. Paspalakis, and G. Juzeliūnas, arXiv:2002.00504v1.

[41] Y. Hong, Z. Wang, D. Ding, and B. Yu, Opt. Express **27**, 29863 (2019).

[42] J. Qiu, Z. Wang, D. Ding, W. Li, and B. Yu, Opt. Express **28**, 2975 (2020).

[43] D. Bortman-Arbiv, A. D. Wilson-Gordon, and H. Friedmann, Phys. Rev. A **63**, 031801(R) (2001).

[44] Z. Amini Sabegh, M. A. Maleki, and M. Mahmoudi, Sci. Rep. **9**, 3519 (2019).

[45] Z. Amini Sabegh, M. Mohammadi, M. A. Maleki, and M. Mahmoudi, J. Opt. Soc. Am. B **36**, 2757 (2019).

[46] J. Ruseckas, A. Mekys, and G. Juzeliūnas, Phys. Rev. A **83**, 023812 (2011).

[47] J. Ruseckas, V. Kudriašov, I. A. Yu, and G. Juzeliūnas, Phys. Rev. A **87**, 053840 (2013).

[48] H. R. Hamedi, J. Ruseckas, and G. Juzeliūnas, Phys. Rev. A **98**, 013840 (2018).

[49] H. R. Hamedi, E. Paspalakis, G. Žlabys, G. Juzeliūnas, and J. Ruseckas, Phys. Rev. A **100**, 023811 (2019).

[50] H. R. Hamedi, J. Ruseckas, E. Paspalakis, and G. Juzeliūnas, Phys. Rev. A **99**, 033812 (2019).

[51] G. Juzeliūnas and P. Öhberg, Phys. Rev. Lett. **93**, 033602 (2004).

[52] G. Juzeliūnas, J. Ruseckas, and P. Öhberg, J. Phys. B: At., Mol. Opt. Phys. **38**, 4171 (2005)

[53] A. J. Menssen, J. Guan, D. Felce, M. J. Booth, and I. A. Walmsley, arXiv:1901.04439.

[54] G. F. Quinteiro and P. I. Tamborenea, Phys. Rev. B **79**, 155450 (2009).

[55] G. F. Quinteiro and T. Kuhn, Phys. Rev. B **90**, 115401 (2014).

[56] K. Köksal and F. Koç, Comput. Theor. Chem. **1099**, 203 (2017).

[57] M. Öncan, F. Koç, D. B. Dereli, and K. Köksal, Comput. Theor. Chem. **1130**, 130 (2018).

[58] M. O. Scully, Phys. Rep. **219**, 191 (1992).

[59] H. S. Borges, L. Sanz, J. M. Villas-Bôas, O. O. Diniz Neto, and A. M. Alcalde, Phys. Rev. B **85**, 115425 (2012).

[60] Z. Dutton and J. Ruostekoski, Phys. Rev. Lett. **93**, 193602 (2004).

[61] M. van Veenendaal and I. McNulty, Phys. Rev. Lett. **98**, 157401 (2007).

[62] G. Donnert, J. Keller, R. Medda, M. A. Andrei, S. O. Rizzoli, R. Lührmann, R. Jahn, C. Eggeling, and S. W. Hell, Proc. Natl. Acad. Sci. USA **103**, 11440 (2006).

[63] A. Mair, A. Vaziri, G. Weihs, and A. Zeilinger, Nature (London) **412**, 313 (2001).

[64] W. M. Lee, B. P. S. Ahluwalia, X.-C. Yuan, W. C. Cheong, and K. Dholakia, J. Opt. A: Pure Appl. Opt. **7**, 1 (2004).

[65] G. J. Beirne, C. Hermannstädter, L. Wang, A. Rastelli, O. G. Schmidt, and P. Michler, Phys. Rev. Lett. **96**, 137401 (2006).

[66] G. J. Beirne, C. Hermannstädter, L. Wang, A. Rastelli, E. Müller, O. G. Schmidt, and P. Michler, Proc. SPIE **6471**, 647104 (2007).

[67] Y. Peng, A. Yang, Y. Xu, P. Wang, Y. Yu, H. Guo, and T. Ren, Sci. Rep. **6**, 38251 (2016).